FREQUENCY-DOMAIN FULL WAVEFORM INVERSION WITH RUGGED FREE SURFACE BASED ON VARIABLE GRID FINITE-DIFFERENCE METHOD

YUANYUAN LI, ZHENCHUN LI, KAI ZHANG and YUZHAO LIN

School of Geosciences, China University of Petroleum, Qingdao 266580, P.R. China.
liyuanyuanlulu@163.com

(Received October 13, 2015; revised version accepted October 4, 2016)

ABSTRACT

Li, Y., Li, Z., Zhang, K. and Lin, Y., 2016. Frequency-domain full waveform inversion with rugged free surface based on variable grid finite-difference method. *Journal of Seismic Exploration*, 25: 543-559.

Full waveform inversion (FWI) is a challenging data-fitting procedure to solve model parameter reconstruction problems. But FWI with irregular topography, which is common in the real land cases, has been barely researched. For more accurately describing of the subsurface structures, we introduce the effect of surface topography in the full waveform inversion. Then we develop a frequency-domain modeling algorithm for irregular topography medium, and incorporate it into a full waveform inversion algorithm. The variable grid finite-difference method is applied to the frequency-domain modeling and inversion algorithm to improve the accuracy of results. Specifically, the computational domain near the surface is discretized by fine rectangular grids, while the rest part is discretized by coarse grids. We apply successive inversions of overlapping frequency groups and layer stripping strategy implemented with complex frequencies to the FWI algorithm to improve the stability of the iterative procedure. In the meantime, the pseudo-Hessian matrix is used to scale the gradient to improve the efficiency. In the numerical tests, we validated our algorithm with two synthetic tests consisting of a layered model and a modified dip section of the overthrust model.

KEY WORDS: full waveform inversion, frequency-domain, variable grid, finite-difference method, rugged free surface.

INTRODUCTION

Full waveform inversion (FWI) is an efficient method to extract quantitative parameter information by the data-fitting between simulated and observed data (Virieux and Operto, 2009). However, the computational cost of forward modeling is one of the most crucial issues in FWI. Recent advances in

0963-0651/16/$5.00

high-performance computing prompt the evolution of FWI to be applied to a more complicated medium, e.g., the elastic medium (Sheen et al., 2006; Prieux et al., 2013; Vigh et al., 2014), the viscoacoustic medium (Hicks and Pratt, 2001; Askan et al., 2007; Smithyman et al., 2009; Malinowski et al., 2011), the anisotropic medium (Lee et al., 2010; Warner et al., 2013; Vigh et al., 2014) and so on. While very few attempts have been performed to reconstruct parameters with the irregular surface by FWI. Moreover, irregular topography is commonly observed in onshore seismic exploration, which has a significant influence on the resolution and accuracy of inversion (Bleibinhaus and Rondenay, 2009). As such, it is essential to perform FWI with surface topography.

The effectiveness of waveform inversion with irregular surface depends on the corresponding modeling algorithm. The forward modeling algorithms with rugged topography have been developed rapidly the in time domain, while the studies for frequency domain are few relatively. Jang et al. (2008) developed a frequency-domain modeling for an irregular surface using the finite-element method (FEM), and incorporated it into an elastic inversion algorithm. Brossier et al. (2008) applied the finite-volume method (FVM) to frequency-domain modeling with the surface topography. Following, a mixed-grid finite element method is presented to simulate seismic wave propagation in complex media (Liu et al., 2014). The main deficiencies of the classical FEM and FVM are the huge memory requirement and the low computational efficiency. By contrast, the finite-difference method (FDM) is most widely used in forward modeling with high efficiency and simplicity. However, the conventional FDM suffers from severe numerical dispersion, when coarse grids are used to discretize the irregular free surface. Robertsson (1996) proposed that a rugged surface should be sampled by at least 15 grid points per minimum wavelength. To balance the artificial diffraction and computational expense, we apply the variable grid FDM (Guo et al., 2014), with fine and coarse rectangular grids to discretize the domain containing the irregular surface and the rest of the model, respectively. And the variable grid FDM has been developed rapidly in time domain (Huang and Dong, 2009). The variable-grid FDM is utilized in frequency domain FWI for the first time.

In addition to the forward modeling with surface topography, an alternative challenging issue is the strong nonlinearity of inversion arising from free-surface multiples (Hicks and Pratt, 2001; Operto et al., 2006). Brossier et al. (2009) implemented two nested hierarchical levels through an outer loop over the slightly overlapping frequency groups and an inner loop over the damping terms to improve the stability of inversion. And the above-mentioned inversion strategies are applied to the inversion algorithm. Moreover, we used pseudo-Hessian matrix to scale the gradient of the misfit function to accelerate convergence (Shin et al., 2001).

First, we introduce the variable grid finite-difference frequency-domain modeling in theory. Second, we describe the theory and strategies of the frequency-domain FWI briefly. And then, we test the FWI method based on the variable grid FDM on a layered model and a modified overthrust model. And last, we present the discussions and conclusions.

FORWARD PROBLEM

The 2D acoustic equation in the time domain (Wei et al., 2014) can be expressed as

$$-[1/(v^2(x,z)][\partial^2 p(x,z,t)/\partial t^2] + (\partial/\partial x)[\partial p(x,z,t)/\partial x] + (\partial/\partial z)[\partial p(x,z,t)/\partial z] = f(x,z,t) \quad . \tag{1}$$

Then we transform eq. (1) into the frequency domain by Fourier transformation, and introduce the complex frequency-shifted perfectly matched layer (CPML) absorbing boundary condition (Zhang and Shen, 2010). Finally, the frequency-domain acoustic wave equation with the CPML absorbing boundary can be written as

$$[\omega^2/v^2(x,z)][p(x,z,\omega)] + (1/s_x)(\partial/\partial x)\{(1/s_x)[\partial p(x,z,\omega)/\partial x]\} + (1/s_z)(\partial/\partial z)\{(1/s_z)[\partial p(x,z,\omega)/\partial z]\} = f(x,z,\omega) \quad . \tag{2}$$

where $p(x,z,\omega)$ is the pressure wavefield in the frequency domain, ω is the angular frequency, $v(x,z)$ is the velocity, s_x and s_z are 1D damping functions for CPML absorbing boundary conditions (Zhang and Shen, 2010), which are shown as follows

$$\begin{aligned} s_x(x) &= \beta_x(x) + \{d_x(x)/[\alpha_x(x) + i\omega]\} \quad , \\ s_z(z) &= \beta_z(z) + \{d_z(z)/[\alpha_z(z) + i\omega]\} \quad , \end{aligned} \tag{3}$$

and $f(x,z,\omega)$ is the source, which is assumed to be known in our inversion algorithm (Liu et al., 2014). Using the mixed-grid finite-difference method (details are given in the Appendix), the acoustic equation can be recast in matrix form (Hustedt et al., 2004)

$$\mathbf{S}\cdot\mathbf{p} = \mathbf{F} \quad , \tag{4}$$

where $\mathbf{S}$ is the impedance matrix depending on medium properties and angular frequency (ω), vector $\mathbf{p}$ and $\mathbf{F}$ of N dimension represent the pressure wavefield and the source term, respectively, where N is the number of the discretized grids.

The rectangular grids are normally used in the mixed-grid finite-difference method. However, the staircase approximation of the irregular surface requires at least 15 points per wavelength, otherwise the artificial diffractions will affect the modeling results. To make a compromise between modeling accuracy and computational cost, we can discretize the domain containing irregular surface by fine grids, while the rest of the model is discretized by coarse grids, as shown in Fig. 1.

In the transition region form fine to coarse grids, the spatial derivative for the coarse grids can be computed directly with the wavefield values around it. However, the derivative for the fine grids cannot be obtained in such a straightforward way as the coarse grids, because the fine grids are not defined below them. Therefore, we have to recur to the interpolation of the wavefield values at coarse grids to estimate the wavefield at the fine grids. In addition to the transition region, the introduction of the stable free-surface boundary condition is critical and difficult in the modeling algorithm. For the implementation of free-surface boundary condition in this study, we map the grid points form Cartesian coordinates to linear coordinates, and set the wavefield of the points above surface zero. We design a simple model to make comparison between variable grid FD and normal coarse grid FD method as shown in Fig. 2. The artificial diffractions can be suppressed visibly by the variable grid FD frequency-domain modeling method.

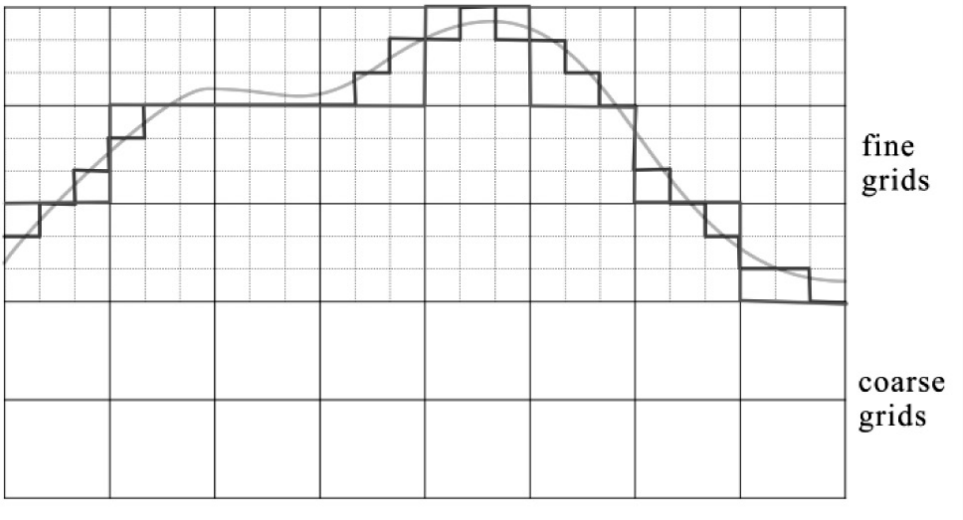

Fig. 1. Strategy of grid discretization for variable grid FD modeling with irregular topography; green curve: the real rugged surface, red curve: the approximation of rugged surface with fine grids for discretization, blue curve: the approximation of rugged surface with coarse grids for discretization.

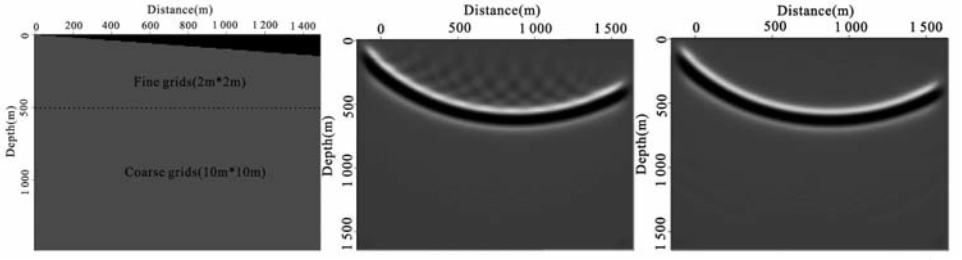

(a) (b) (c)

Fig. 2. Snapshots computed with variable grid (c) and normal coarse grid (b) finite-difference frequency-domain modeling for the model (a).

INVERSE PROBLEM

Full waveform inversion is a numerical optimization problem with an attempt to minimize the misfit between the recorded and modeled wavefields (Tarantola, 1984). The objective function [E(**m**)] in the frequency domain waveform inversion (Brossier et al., 2009) can be given as

$$E(\mathbf{m}) = \tfrac{1}{2}(\mathbf{S}_d\Delta\mathbf{d})^{\dagger}(\mathbf{S}_d\Delta\mathbf{d}) = \tfrac{1}{2}\Delta\mathbf{d}^{\dagger}\mathbf{S}_d^{\dagger}\mathbf{S}_d\Delta\mathbf{d} = \tfrac{1}{2}\Delta\mathbf{d}^{\dagger}\mathbf{W}_d\Delta\mathbf{d} \quad , \tag{5}$$

where **m** is the model parameter, $\Delta\mathbf{d}$ is the residual wavefield, '†' denotes the conjugate transpose of the vector, $\mathbf{W}^{\dagger} = \mathbf{S}_d^{\dagger}\mathbf{S}_d$ is the weighted operator and $\mathbf{S}_d$ is the diagonal weighting matrix to scale the relative contributions of each component of the residual wavefield vector.

The gradient used in the inversion algorithm can be obtained by minimizing the objective function. In its standard form,the gradient is given by (Brossier et al., 2009)

$$\nabla_m E = \Re\{\mathbf{J}^{t}\mathbf{W}_d\Delta\mathbf{d}^*\} \quad , \tag{6}$$

where $\nabla_m E$ is the gradient of objective function, $\Re$ denotes the real part of a complex number, **J** is the Jacobian matrix, 't' denotes the transpose of the matrix, and $\Delta\mathbf{d}^*$ is the conjugate of the residual wavefield vector. The Jacobian matrix can be written as

$$\mathbf{J} = \mathbf{S}^{-1}\mathbf{F}_v \quad , \tag{7}$$

where

$$\mathbf{F}_v = [-(\partial\mathbf{S}/\partial m_1)\mathbf{p} \quad -(\partial\mathbf{S}/\partial m_2)\mathbf{p} \quad \cdots \quad -(\partial\mathbf{S}/\partial m_n)\mathbf{p}] \quad . \tag{8}$$

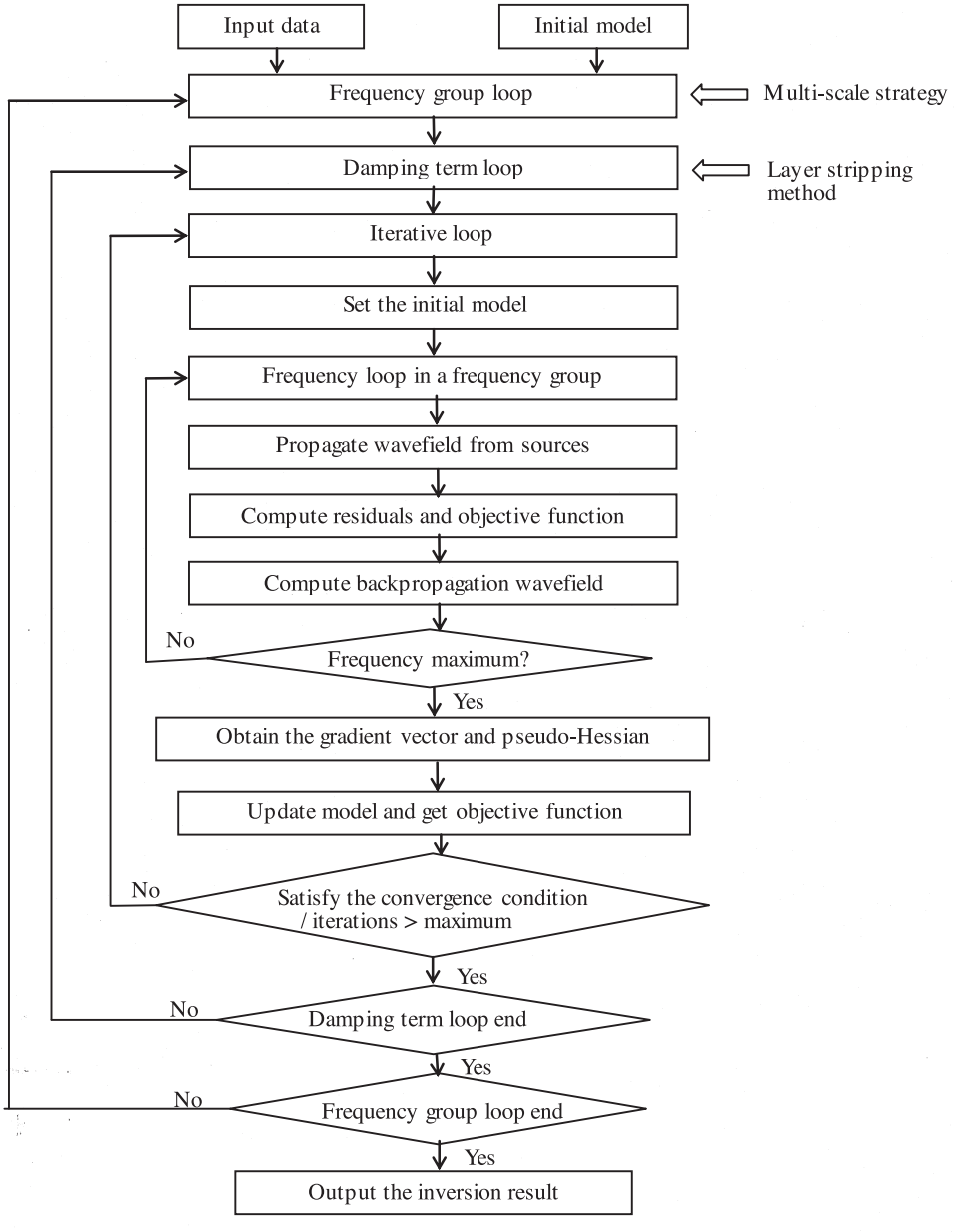

Fig. 3. The flow chart of inversion algorithm used in this study.

Considering the strong nonlinearity caused by the surface effect, some scaling and regularizations should be applied to the gradient to obtain stable and reliable results. Besides, the pseudo-Hessian matrix and a 2D Gaussian smooth regularization operator is used to scale the gradient properly. The correlation lengths of Gaussian spatial filter should be adapted to the inversion frequency (Ravaut et al., 2004). The formula used in the inversion algorithm can be shown as

$$\begin{aligned}\mathbf{m} &= \mathbf{m}_0 - \alpha(\mathbf{H}_{\text{pseudo}} + \lambda\mathbf{I})^{-1}\mathbf{G}_s\nabla_m E \\ &= \mathbf{m}_0 - \alpha(\mathbf{H}_{\text{pseudo}} + \lambda\mathbf{I})^{-1}\mathbf{G}_s\Re(\mathbf{J}^T\mathbf{W}_d\Delta\mathbf{d}^*) \quad , \end{aligned} \tag{9}$$

where $\mathbf{m}_0$ is the starting model, $\mathbf{m}$ is the updated model, α is a step length, $\mathbf{H}_{\text{pseudo}}$ is the pseudo-Hessian matrix (Shin et al., 2001), λ is the damping factor to avoid numerical instability (i.e., division by zero), $\mathbf{G}_s$ refers to the Gaussian smoothing term.

We applied the multiscale FWI scheme in the inversion algorithm. Owing to the irregular surface effects, the robustness of inversion is poorer. The multiscale inversion is based on successive inversions of slightly overlapping frequency groups. Besides, the stability of FWI can be improved by the layer stripping method which can be realized by complex frequency. The relative contributions of the arrivals from shallow layers will be increased by damping the seismograms in time, and it is helpful for the reconstruction of shallow layers. The velocity will be inverted effectively in the layer-stripping mode by adjusting the damping term (i.e., the imaginary part of complex frequency). The detailed description of our inversion algorithm is shown in Fig. 3 as follows. Two nested hierarchical levels through an outer loop over the slightly overlapping frequency groups and an inner loop over the damping terms are used in the FWI algorithm to improve the stability of inversion (Brossier et al., 2009).

NUMERICAL EXAMPLES

Four layered model with anomalies test

A four layered media with a rugged free surface (including peaks and valleys) and two anomalies (Fig. 4) is used to test the effect of irregular topography and the accuracy of the inversion algorithm. The size of the model is 151×101 grid nodes with a regular spacing of 12 m.

There are 50 shots located 12 m below the rugged surface, with a horizontal spacing of 36 m. Every shot is recorded by 151 receivers located on the surface, with a horizontal spacing of 12 m. The source is a Ricker wavelet with a dominant frequency of 10 Hz. To improve the accuracy of modeling with

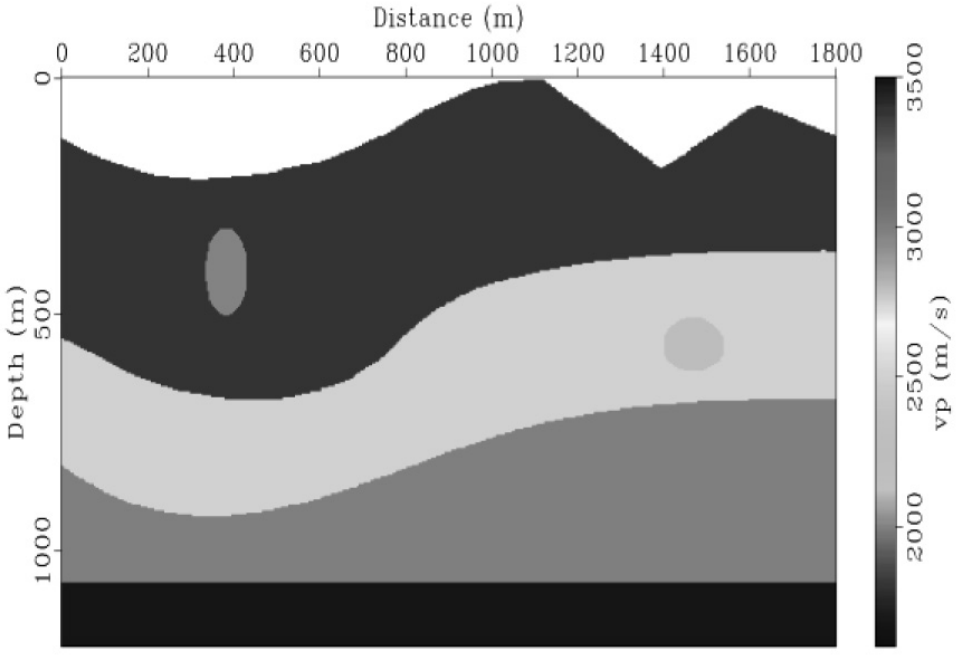

Fig. 4. True model for the synthetic four layered model test.

the rugged surface, we implement variable grid technique. The domain including the surface (i.e., the domain above the depth of 248 m) is discretized by fine grids with a spacing of 4 m, while the rest part is discretized by coarse grids with a spacing of 12 m. The satisfactory result of modeling is achieved without obvious artificial wave phenomenon as shown in Fig. 5a. The shot records appear strongly scattered owing to the rugged surface, and comprise reverberations. Besides, the events are distorted seriously.

To verify that the rugged free surface has great influence on the seismic data and inversion result, we also simulated shot records for the true model with an absorbing boundary and a flat free surface boundary on top, respectively, which are shown in Figs. 5b and 5c. Because the surface of the model is flat, the shots are located at depth of 12 m, and the receivers are laid on the surface. Besides, all the other parameters used during the simulation are the same as those used for four layered model with the rugged free surface. The obvious surface multiples are shown in Fig. 5c because of the flat free surface. The irregular surface leads to the serious distortions of events and apparent scattered waves by comparison between the seismograms with rugged free surface and that with flat free surface. On the whole, a comparison between the simulated seismograms with different boundary conditions shows that the shot records with rugged free surface is the most complicated. We try to implement the inversion

algorithm under the assumption of flat free surface for the seismic data with rugged surface, but the recovered model converges badly. In conclusion, the effect of rugged free surface on simulated seismograms and inverted result is important and worthy of consideration. In the next section, we will introduce the process and the result of FWI with rugged surface.

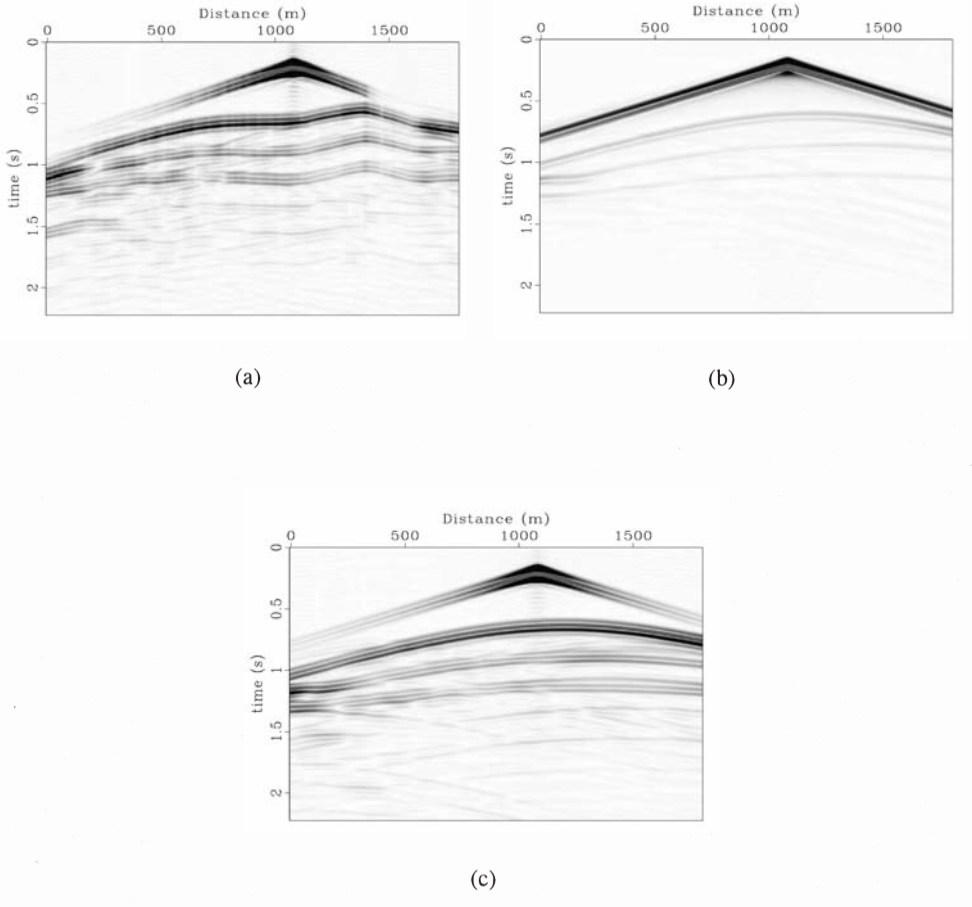

Fig. 5. Seismograms computed with finite-difference frequency-domain code for true model with a rugged free surface (a), an absorbing surface (b) and a flat free surface (c) on top. The shot is located at x = 1080 m.

The initial model was a filtered version of the true model without anomalies as shown in Fig. 6a. The source signature was assumed to be known in the inversion algorithm. To avoid the convergence to the local minimum, four frequency groups were used for inversion successively with three frequencies

per group, namely, (7, 8, 9) Hz, (11, 12, 13) Hz, (16, 17, 18) Hz and (21, 22, 23) Hz. The inversion was performed without damp terms to precondition the seismic data, because the model is relatively simple. When the maximum iteration of 40 for each frequency group is reached or the convergence criterion is satisfied ($|\mathrm{E}(\mathbf{m})_{\mathrm{iter}} - \mathrm{E}(\mathbf{m})_{\mathrm{iter}-1}| < \mathrm{E}(\mathbf{m})_{\mathrm{iter}-1} \times 1 \times 10^{-5}$), the loop over the inversion iterations of one frequency group is stopped. The final inversion result is shown in Fig. 6b. The two anomalies and the interface between layers are reconstructed successfully. A comparison between vertical profiles of the inverted model, the true model and the initial model shows a reliable estimate of velocity (Fig. 7).

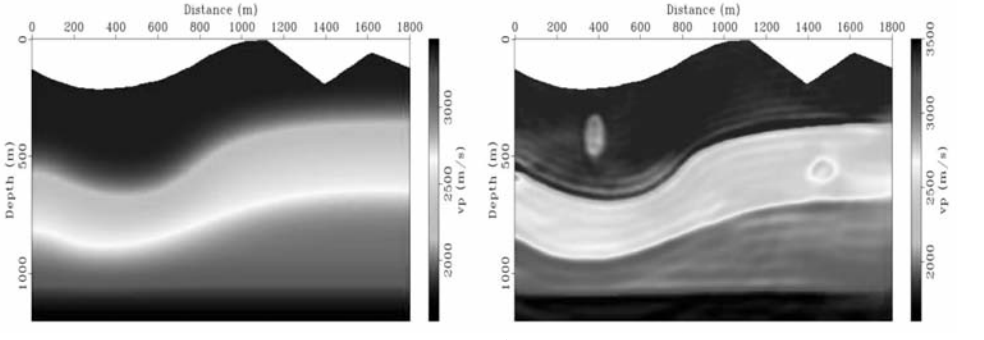

(a) (b)

Fig. 6. Initial (a) and inverted (b) model for the synthetic four layered model test.

Modified overthrust model test

We tested our FWI algorithm by an irregular surface model which is a modified version of a dip section of the SEG/EAGE overthrust model (Fig. 8a). The size of model is 600×140 grid nodes with a regular spacing of 25 m.

149 shots are laid 25 m below the irregular surface, with a horizontal interval of 100 m. There are 600 receivers located on the surface with a horizontal interval of 25 m. The synthetic seismograms are generated by the finite-difference frequency-domain modeling algorithm with irregular topography using variable grid method. The domain including the surface (i.e., the domain above the depth of 500 m) is discretized by fine grids with a spacing of 5 m, while the rest of the model is discretized by coarse grids with a spacing of 25m. Fig. 9 shows the synthetic seismograms for the 74th shot using the Ricker wavelet with the dominant frequency of 8 Hz as source wavelet. As shown in Fig. 9, artificial reflections or diffractions are almost invisible, and the relatively accurate result is owing to the implementation of variable grid technique with fine rectangle grids to approximate the irregular surface.

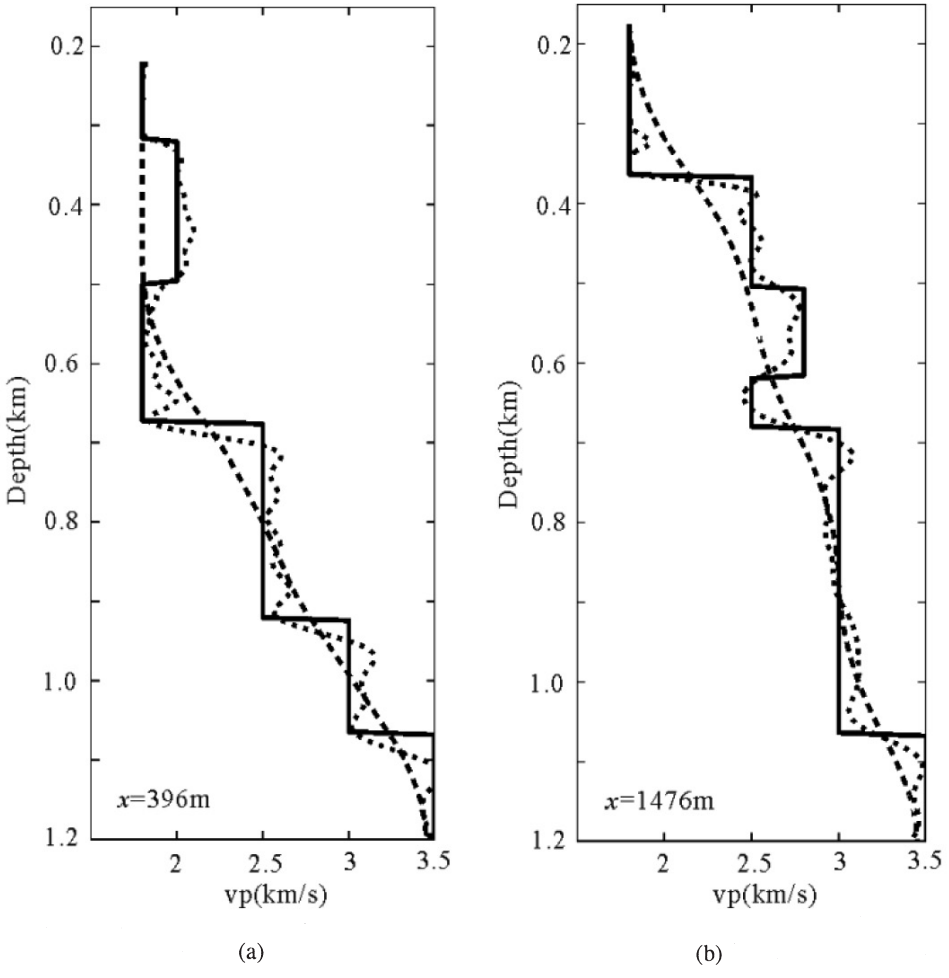

Fig. 7. Vertical profiles for the velocity parameter at x = 396 m (a), and x = 1476 m (b). Profiles of the true, the initial and the inverted models are plotted with solid, dashed and dotted lines, respectively.

The initial velocity model for inversion was acquired by smoothing the true model with a Gaussian function of vertical and horizontal correlation ranges of 400 m (Fig. 8b). Four overlapping frequency groups were inverted successively with four frequencies per group, namely, (3, 3.5, 4, 4.5) Hz, (4, 4.5, 5, 6) Hz, (5, 6, 7, 8) Hz, and (7, 8, 9, 10) Hz. Besides, four damping factors (i.e., 1.5, 1.0, 0.5 and 0.02) were used to improve the stability of inversion. The maximum number of iterations is still 40 for each complex-valued frequency group, and the convergence criterion is same as that of the inversion for the four layered model. The velocity model recovered with the inversion schemes is shown in Fig. 10. Fig. 11 shows the vertical profiles of the

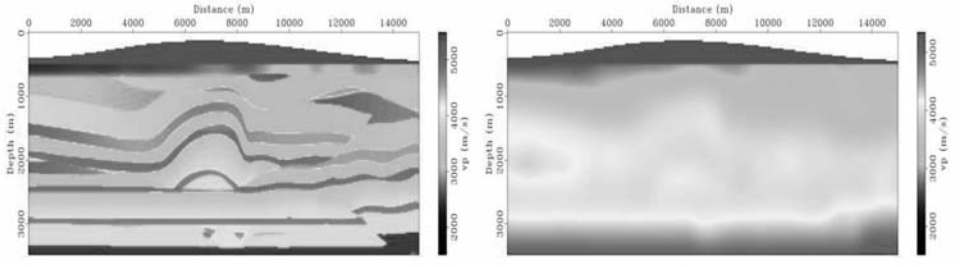

(a) (b)

Fig. 8. True (a) and initial (b) model for the synthetic modified overthrust model test.

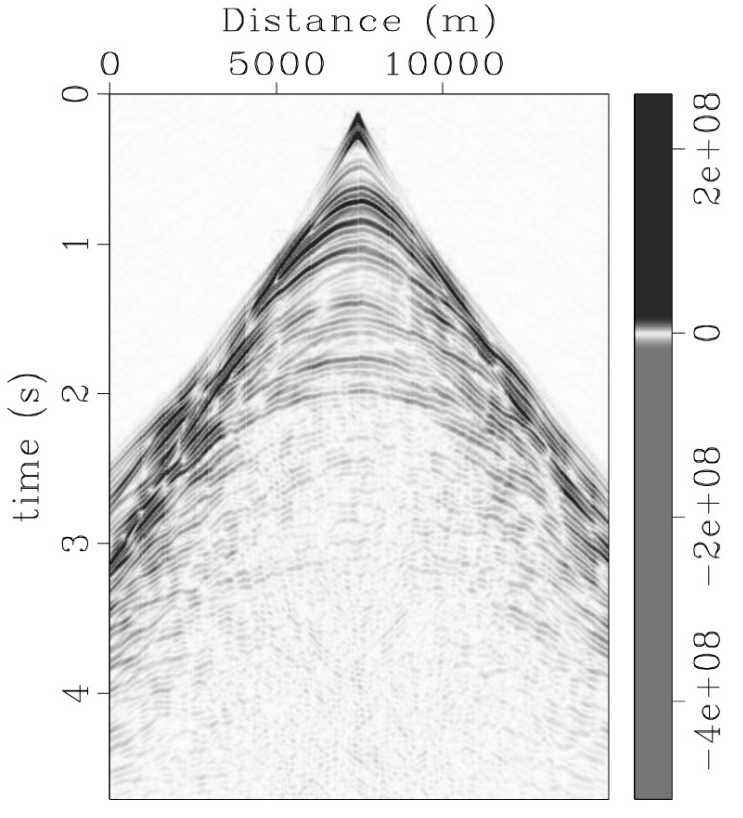

Fig. 9. Seismograms computed with finite-difference frequency-domain code for true model with a rugged free surface on top. The shot is located at x = 7450 m.

recovered velocity model at a distance of 7200 m and 12 km. The shallow part of recovered velocity is closer to the true velocity model than the deep part, which is because of the influence of illumination and surface multiples. Synthetic seismograms for the inverted velocity model and the misfit between seismograms for the true velocity and that for the inverted velocity model are shown in Fig. 12. We can see that the two synthetic seismograms fit well. On the whole, the velocity model can be recovered reasonably with the frequency domain inversion scheme, when the irregular surface is present.

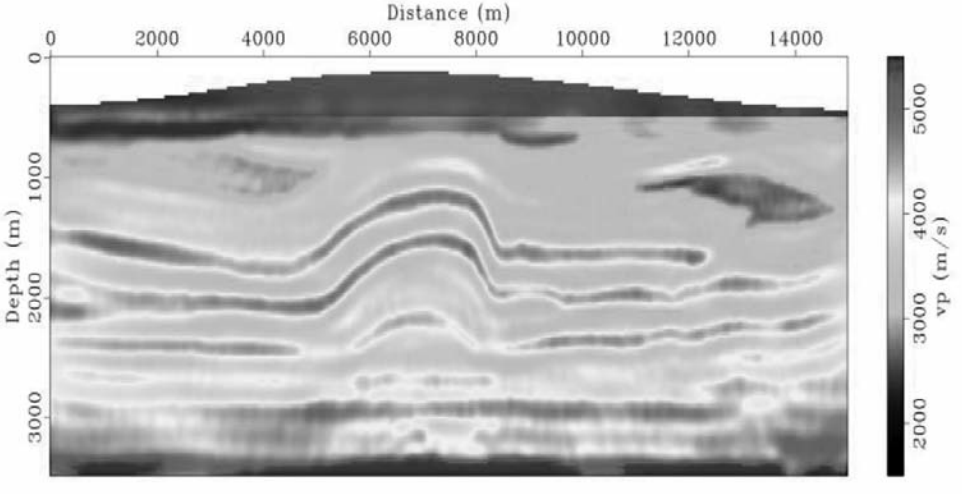

Fig. 10. The inversion result.

CONCLUSIONS

Our study develops a variable grid finite-difference frequency-domain modeling with surface topography and the corresponding inversion schemes. By grid refinement near the irregular surface, we can efficiently simulate the wave propagation for surface topography without apparent artificial wave phenomenon. The modeling algorithm is incorporated into a full waveform inversion algorithm for the first time. Considering the increased nonlinearity produced by the effect of complex topography, two-level multi-scale strategy implemented with successive inversions of overlapping frequency groups and damping terms is critical to recover the velocity model stably. Besides, the pseudo-Hessian matrix is used to scale the gradient of objective function to improve the convergence. The frequency-domain inversion algorithm proves to be effective for the complex model with surface topography by numerical tests.

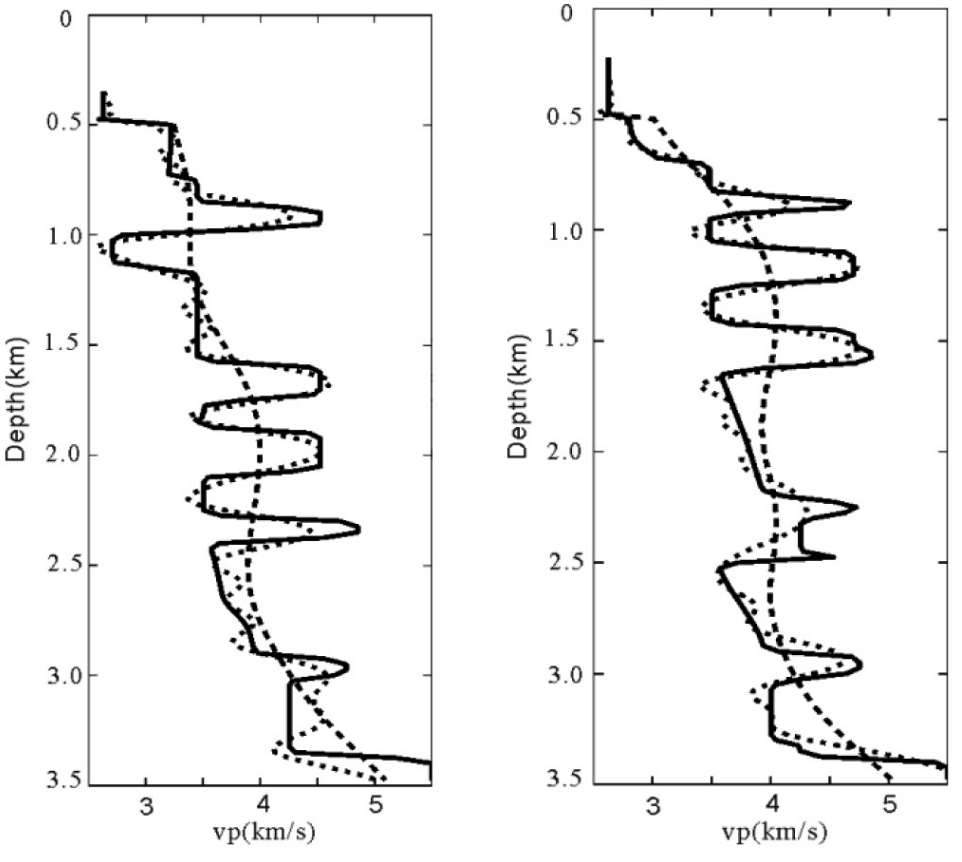

Fig. 11. Vertical profiles for the velocity parameter at x = 7.2 km (a) and x = 12 km (b). Profiles of the true, the initial and the inverted models are plotted with solid, dashed and dotted lines, respectively.

ACKNOWLEDGEMENTS

Thanks to Zhenbo Guo for the helpful discussions and suggestions about the paper. This research is supported by SWPI laboratory at CUP. This research is supported by China NSF grant (41374122, 41504100), Shandong Provincial NSF (ZR2013DL012), and Fundamental Research Funds for the Central Universities (16CX06039A). The comments provided by the anonymous reviewer were extremely helpful and led to significant improvements in the quality of the manuscript.

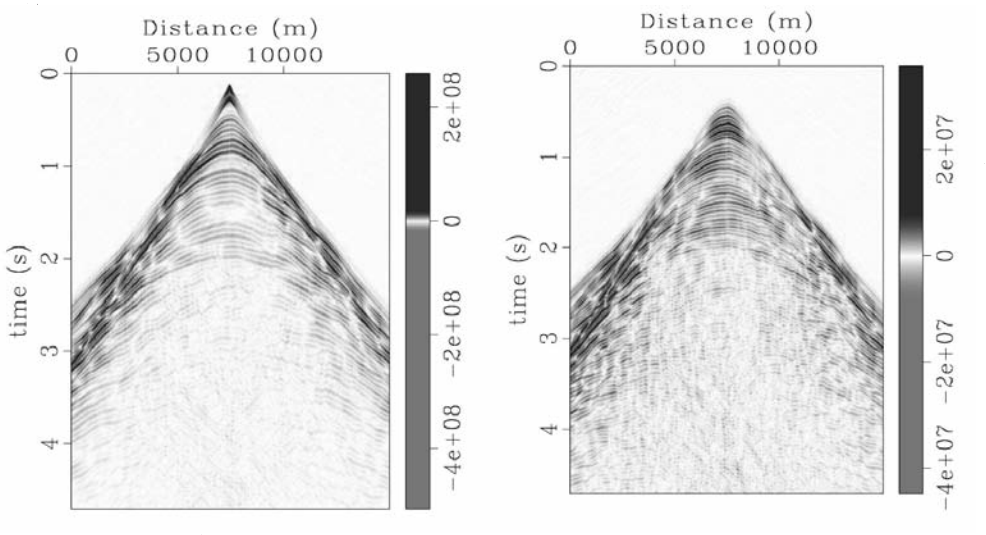

(a) (b)

Fig. 12. Synthetic seismograms for the inverted velocity model (a) and the misfit between synthetic seismograms for the true velocity model and that for the inverted velocity model (b).

REFERENCES

Askan, A., Akcelik, V., Bielak, J., and Ghattas, O., 2007. Full waveform inversion for seismic velocity and anelastic losses in heterogeneous structures. Bull. Seismol. Soc. Am., 97: 1990-2008.

Bleibinhaus, F. and Rondenay, S., 2009. Effects of surface scattering in full-waveform inversion. Geophysics, 74: WCC69-WCC77.

Brossier, R., Virieux, J. and Operto, S., 2008. Parsimonious finite-volume frequency-domain method for 2-D P-SV-wave modeling. Geophys. J. Internat., 175: 541-559.

Brossier, R., Operto, S. and Virieux, J., 2009. Seismic imaging of complex onshore structures by 2D elastic frequency-domain full-waveform inversion. Geophysics, 74: WCC105-WCC118.

Guo, Z.B., and Li, Z.C., 2014. Acoustic wave modeling in frequency-spatial domain with surface topography. J. Jilin Univ. (Earth Sci. Ed.), 44: 683-693.

Hicks, G.J. and Pratt, R.G., 2001. Reflection waveform inversion using local descent methods: estimating attenuation and velocity over a gas-sand deposit. Geophysics, 66: 598-612.

Huang, C., and Dong, L.G., 2009. Staggered-grid high-order finite-difference method in elastic wave simulation with variable grids and local time-steps. Chin. J. Geophys., 52: 2870-2878. (in Chinese)

Hustedt, B., Operto, S. and Virieux, J., 2004. Mixed- grid and staggered-grid finite-difference methods for frequency-domain acoustic wave modeling. Geophys. J. Internat., 157: 1269-1296.

Jang, U., Min, D., Choi, Y. and Shin, C., 2008. Frequency-domain elastic waveform inversion with irregular surface topography. Expanded Abstr., 78th Ann. Internat. SEG Mtg., Las Vegas: 1-5.

Lee, H.-Y., Koo, J.M., Min, D.-J., Kwon, B.-D. and Yoo, H.S., 2010. Frequency-domain elastic full waveform inversion for VTI media. Geophys. J. Internat., 183: 2884-2904.

Liu, C., Gao, F.X., Feng, X., Liu, Y. and Ren, Q.C., 2015. Memoryless quasi-Newton (MLQN) method for 2D acoustic full waveform inversion. Explor. Geophys., 46: 168-177.

Liu, X.X., Yin, X.Y. and Li, H.S., 2014. Optimal variable-grid finite-difference modeling for porous media. J. Geophys. Engineer., 11: 65011-65019.

Malinowski, M., Operto, S. and Ribodetti, A., 2011. High-resolution seismic attenuation imaging from wide-aperture onshore data by visco-acoustic frequency-domain full-waveform inversion. Geophys. J. Internat., 186: 1179-1204.

Operto, S., Virieux, J., Dessa, J.X. and Pascal, G., 2006. Crustal seismic imaging from multifold ocean bottom seismometer data by frequency domain full waveform tomography: Application to the eastern Nankai trough. J. Geophys. Res., 111: B09306.

Prieux, V., Brossier, R., Operto, S. and Virieux, J., 2013. Multiparameter full waveform inversion of multicomponent ocean-bottom-cable data from the Valhall field. Part 1: Imaging compressional wave speed, density and attenuation. Geophys. J. Internat., 194: 1640-1664.

Ravaut, C., Operto, S., Improta, L., Virieux, J., Herrero, A. and Dell'Aversana, P., 2004. Multiscale imaging of complex structures from multifold wide-aperture seismic data by frequency-domain full-waveform tomography: application to a thrust belt. Geophys. J. Internat., 159: 1032-1056.

Robertsson, J.O.A., 1996. A numerical free-surface condition for elastic/viscoelastic finite-difference modeling in the presence of topography. Geophysics, 61: 1921-1934.

Sheen, D.H., Tuncay, K., Baag, C.E. and Ortoleva, P.J., 2006. Time domain Gauss-Newton seismic waveform inversion in elastic media. Geophys. J. Internat., 167: 1373-1384.

Shin, C., Yoon, K., Marfurt, K.J., Park, K., Yang, D., Lim, H.Y., Chung, S., and Shin, S., 2001. Efficient calculation of a partial-derivative wavefield using reciprocity for seismic imaging and inversion. Geophysics, 66: 1856-1863.

Smithyman, B., Pratt, R.G., Hayles, J. and Wittebolle, R., 2009. Detecting near-surface objects with seismic waveform tomography. Geophysics, 74: WCC119-WCC127.

Tarantola, A., 1984. Linearized inversion of seismic reflection data. Geophys. Prosp., 32: 998-1015.

Vigh, D., Cheng, X., Jiao, K., Sun, D. and Kapoor, J., 2014. Multiparameter TTI full waveform inversion on long-offset broadband acquisition: A case study. Expanded Abstr., 84th Ann. Internat. SEG Mtg., Denver: 1-5.

Warner, M., Ratcliffe, A., Nangoo, T., Morgan, J., Umpleby, A., Shah, N., Vinje, V., Štekl, I., Guasch, L., Win, C., Conroy, G. and Bertrand, A., 2013. Anisotropic 3D full-waveform inversion. Geophysics, 78: R59-R80.

Wei, Z.F., Gao, H.W. and Zhang, J.F., 2014. Time-domain full waveform inversion based on an irregular-grid acoustic modeling method. Chin. J. Geophys., 57: 586-594.

Zhang, W. and Shen, Y., 2010. Unsplit complex frequency-shifted PML implementation using auxiliary differential equations for seismic wave modeling. Geophysics, 75: T141-T154.

APPENDIX

MIXED-GRID FINITE DIFFERENCE MODELING

The numerical dispersion is most significant along the bisectrices when a standard five-point stencil (x - z or x′ - z′ coordinate system as shown in Fig. A-1) is used in the finite difference modeling. The mixed-grid finite difference scheme (Fig. A-1) is applied to reduce the numerical dispersion. A combination of two staggered-grid stencils on the classical Cartesian coordinate system (x - z coordinate system as shown in Fig. 13) and the 45° rotated

coordinate system (x′ - z′ coordinate system as shown in Fig. A-1) is the basis of the mixed-grid stencil. The spatial derivative is approximated by linearly combining two discretizations of the derivative operator on the x - z coordinate system and the x′ - z′ coordinate system. The mass acceleration term should be approximated by using a weighted average over the nine nodes included in mixed-grid operator stencil (Fig. A-1), as is done in finite-element modeling. Then, the weighting coefficients should be obtained by optimization method that minimizes the dispersion.

The discretized form of frequency-domain acoustic wave equation [eq.(2)] based on mixed-grid finite difference scheme is

$$C_1 p_{i,j} + C_2 p_{i+1,j} + C_3 p_{i-1,j} + C_4 p_{i,j-1} + C_5 p_{i,j+1}$$

$$+ R_1 p_{i-1,j-1} + R_2 p_{i+1,j-1} + R_3 p_{i-1,j+1} + R_4 p_{i+1,j+1} = f_{i,j} \quad . \qquad \text{(A-1)}$$

where $p_{i,j}$ is the pressure wavefield at the node (i,j), C_i and R_i are the coefficients defined by medium parameters, optimized weighting coefficients, difference coefficients and so on, $f_{i,j}$ is the source term. And finally, eq. (A-1) can be recast into the matrix-type equation as shown in eq. (4).

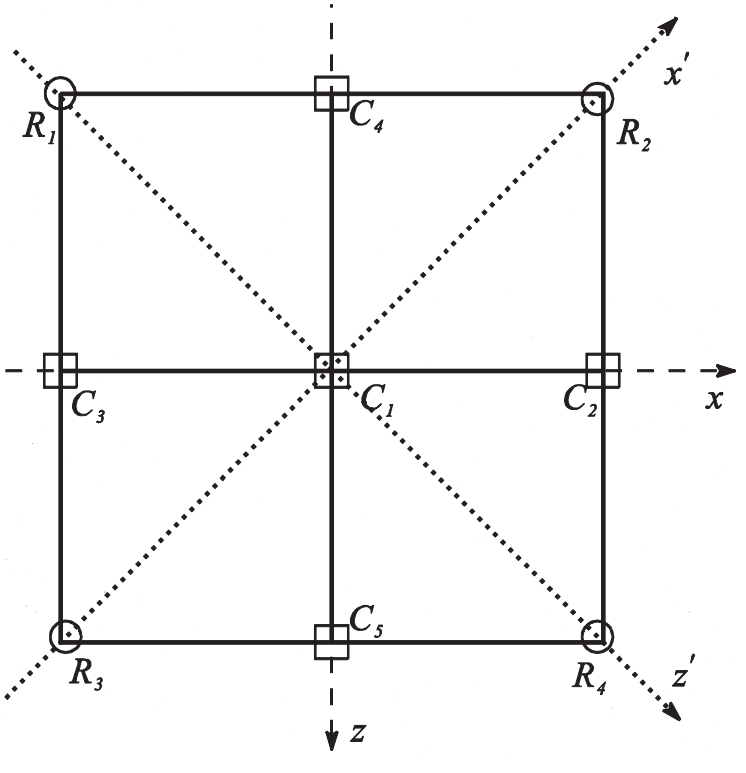

Fig. A-1. Mixed-grid finite difference scheme.